Approximation of Quantities of Interest in stochastic PDEs by the random discrete L2 projection on polynomial spaces

MIGLIORATI, G.;NOBILE, F.;VON SCHWERIN, E.;TEMPONE, R.

Approximation of Quantities of Interest in stochastic PDEs by the random discrete L^2 projection on polynomial spaces

G. Migliorati*†   F. Nobile*†   E. von Schwerin†   R. Tempone‡

November 27, 2012

Abstract

In this work we consider the random discrete L^2 projection on polynomial spaces (hereafter RDP) for the approximation of scalar Quantities of Interest (QOIs) related to the solution of a Partial Differential Equation model with random input parameters. The RDP technique consists of randomly sampling the input parameters and computing the corresponding values of the QOI, as in a standard Monte Carlo approach. Then, the QOI is approximated as a multivariate polynomial function of the input parameters by a discrete least squares approach.

We consider several examples including the Darcy equations with random permeability; the linear elasticity equations with random elastic coefficient; the Navier-Stokes equations in random geometries and with random fluid viscosity.

We show that the RDP technique is well suited for QOIs that depend smoothly on a moderate number of random parameters. Our numerical tests confirm the theoretical findings in [14], which have shown that, in the case of a single random parameter uniformly distributed, the RDP technique is stable and optimally convergent if the number of sampling points scales quadratically with the dimension of the polynomial space. However, in the case of several random input parameters, numerical evidence shows that this condition could be relaxed and a linear scaling seems enough to achieve stable and optimal convergence, making the RDP technique very promising for high dimensional uncertainty quantification.

Keywords: PDE stochastic data, polynomial approximation, discrete least squares.

AMS Subject Classification: 41A10, 65N35.

1   Introduction

In the last years, the modeling of uncertainty in mathematical models has attracted a lot of attention in the scientific community. When a probabilistic framework is considered, uncertainty in the model parameters is modeled in terms of random variables. The

---

*MOX-Dipartimento di Matematica "Francesco Brioschi", Politecnico di Milano, Italy.
†MATHICSE-CSQI, EPF de Lausanne, Switzerland.
‡Applied Mathematics and Computational Sciences, KAUST, Thuwal, Saudi Arabia.
giovanni.migliorati@gmail.com , raul.tempone@kaust.edu.sa

underlying challenge concerns the accurate and efficient approximation of the model outcome in presence of many random input parameters. In the context of PDE's with stochastic data, a well-established technique that has been employed in many engineering applications [8, 12, 9] consists in the use of a spectral expansion to represent the input/output dependence; see e.g. [10, 16, 13]. Once such an expansion has been computed by some means, statistics of the model output can be easily recovered. The *random discrete L^2 projection* (RDP), also known as regression or point collocation approach, has been proposed in the context of applications devoted to uncertainty analysis in [12, 3, 7] as a tool to compute the spectral expansion of the model response. The regression approach is based on the evaluation of the target output function on randomly selected points, and aims to improve the slow convergence of the classical Monte-Carlo method by performing a discrete projection onto a multivariate polynomial space. It differs from other techniques based on a deterministic choice of the points where to evaluate the function, also known as *Collocation methods on Sparse Grids* [4].

In [14, 5] the RDP was analyzed in the context of approximating a smooth aleatory function in the L^2 probability sense. This approximation problem falls in the field of non-parametric regression with random design, and when noise is present there exist well-known estimates for the approximation error [11]. The RDP of a given aleatory function, consists in its discrete L^2 projection over a polynomial space, and is computed evaluating the target function point-wise in randomly selected points of the parameter space. The evaluations are assumed to be noise-free. The stability and convergence properties of RDP are analyzed in [14, 5]. Under some assumptions on the probability density, it is proved in these works that, in one dimension and when the number of sampling points scales quadratically with respect to the dimension of the polynomial space, the RDP converges at the optimal convergence rate, *i.e.* the error is equivalent up to a constant to the best approximation error of the target function in the chosen polynomial space. Several numerical tests show the capabilities of the method, and highlight the influence of the dimension of the parameter space and of the smoothness of the target function on the achieved convergence rate.

The present work focuses on the application of RDP to the approximation of quantities of interest related to the solution of PDEs with stochastic data. The aleatory function is defined as an integral of the solution of the PDE over a portion of the physical domain. We begin by considering the Darcy model with a random diffusion coefficient, parametrized in a one-dimensional parameter space. The randomness affects the value of the coefficient in a particular region of the physical domain, for instance an inclusion. Then we investigate the same example, but when the randomness affects the location where the diffusion coefficient is discontinuous. In particular, this example treats an inclusion with a random domain, *i.e.* the geometrical shape of the domain is parametrized in terms of a random variable.

Next, we move to higher dimensional parameter spaces, always choosing the polynomial space to be the isotropic Total Degree space. This choice is well motivated in those cases where the target function depends analytically on each input parameter with analyticity region not affected by the other parameters [2]. We consider a Darcy model with a random diffusion coefficient parametrized in a five-dimensional parameter space, increasing the number of nonoverlapping inclusions that are displaced in the physical domain to five.

Lastly, we consider two more complex vectorial problems: the Navier-Lamé equations that govern the bending of a cantilever beam in the regime of linear elasticity, and the incompressible Navier-Stokes equations that govern the motion of a viscous fluid in a pipe. Both examples contain uncertainty in the model parameters: the Young modulus

in the former, and the viscosity and the geometry of the domain in the latter.

All examples of the elliptic class presented in this paper, with one-dimensional parameter space, validate the theoretical results outlined in [14, 5]. In particular, a number of sampling points proportional to the square of the dimension of the polynomial space always yields optimal convergence, as predicted by the theory. Moreover, when the function to approximate is smooth, an optimal convergence is observed up to a certain threshold, even if the number of sampling points is only linearly proportional to the dimension of the polynomial space. Beyond such threshold, the error starts diverging. The same holds in higher dimensional parameter spaces. As pointed out in [14], when the dimension gets higher, the sample points naturally spread over the whole parameter space, and the RDP becomes more stable even when the number of sample points is only linearly proportional to the dimension of the polynomial space. In this case optimal convergence rate for smooth functions has always been achieved, in all ranges of polynomial space dimensions tested (*i.e.* no blow up has been observed).

The previous give indications on the correct amount of "regularization" needed to achieve the optimal convergence rate, that is how much smaller the number of degrees of freedom necessary to parametrize the polynomial space has to be with respect to the number of sampling points. In this sense, the one-dimensional case is the most ill-conditioned case, making the RDP more promising in high dimensional approximation problems.

The outline of the paper is the following: in Section 2 we introduce the formulation of the random discrete L^2 projection and recall the main results obtained in [14] concerning stability and optimality. In Section 3 the numerical examples are presented. Examples 1,2,3 are based on the Darcy model with random permeability. Example 4 and 5 address the linear elasticity equations with random elastic coefficient, and Navier-Stokes equations in random geometries and with random fluid viscosity. Finally, in Section 4 we draw some conclusions.

2   The random discrete L^2 projection on polynomial spaces

In this section, we review in abstract settings the formulation of the random discrete L^2 projection and recall the main results obtained in [14]. The technique will then be applied to PDEs with random data in Section 3.

Let $\Gamma \subseteq \mathbb{R}^N$ be an N-dimensional subset of the N-dimensional Euclidean space, with a tensor structure form $\Gamma = \Gamma^1 \times \cdots \times \Gamma^N$. Denote by $\rho : \Gamma \to \mathbb{R}^+$ a probability density function over Γ, and by $\mathbf{Y} = (Y_1, \ldots, Y_N)$ a vector of N random variables, taking values in Γ and distributed according to the density ρ.

We consider a random variable $Z = \phi(\mathbf{Y})$, where $\phi : \Gamma \to \mathbb{R}$ is assumed to be a smooth function, and we are interested in computing statistical moments of Z. This will be achieved by first constructing a reduced model; i.e. we approximate the function $\phi(Y_1, \ldots, Y_N)$ by a suitable multivariate polynomial $\phi_\Lambda(Y_1, \ldots, Y_N)$. We then compute statistical moments using the approximate function ϕ_Λ.

We denote by

$$\mathbb{E}[Z] := \int_\Gamma \phi(\mathbf{Y})\rho(\mathbf{Y})d\mathbf{Y}$$

the expected value of the random variable $Z = \phi(\mathbf{Y})$ and by

$$P(A) := \int_A \rho(\mathbf{Y})d\mathbf{Y}$$

the probability of the event $A \in \mathcal{B}(\Gamma)$, where $\mathcal{B}(\Gamma)$ is the Borel σ-algebra with respect to the measure $\rho(\mathbf{Y})d\mathbf{Y}$. Throughout the paper we also assume that:

Assumption 1 Γ *is a bounded set, and* $0 < \rho_{min} \leq \rho(\mathbf{y}) \leq \rho_{max} < \infty$, $\forall \mathbf{y} \in \Gamma$.

Remark 1 *This assumption excludes* e.g. *the normal and lognormal cases, since these densities are not bounded away from zero due to their unbounded support. Assumption 1 is needed only in the proof of Theorem 2 (see Section 2.2). The Propositions 2, 1 and Theorem 1 hold also with the normal and lognormal densities. The proofs of these results are presented in [14].*

We introduce the space L_ρ^2 of square integrable functions $f : \Gamma \to \mathbb{R}$, endowed with the norm

$$\|f\|_{L_\rho^2} = \left(\int_\Gamma f^2(\mathbf{Y})\rho(\mathbf{Y})d\mathbf{Y} \right)^{1/2}.$$

Let $\mathbf{p} = (p_1, \ldots, p_N)$ be a multi-index and $\Lambda \subset \mathbb{N}^N$ a set of multi-indices. In the sequel we consider only sets Λ that are monotone in the following sense:

Property 1 (Monotonicity of Λ) *Consider two multi-indices* $\mathbf{p}', \mathbf{p}'' \in \mathbb{N}^N$ *such that* $p_n'' \leq p_n'$, $\forall n = 1, \ldots, N$. *The multi-index set Λ is monotone if the following holds:*

$$\mathbf{p}' \in \Lambda \Longrightarrow \mathbf{p}'' \in \Lambda.$$

We denote by $\mathbb{P}_\Lambda(\Gamma)$ the multivariate polynomial space

$$\mathbb{P}_\Lambda(\Gamma) = \mathrm{span}\left\{ \prod_{n=1}^N y_n^{p_n}, \text{ with } \mathbf{p} \in \Lambda \right\}, \tag{1}$$

and by $\#\Lambda = dim(\mathbb{P}_\Lambda)$ the dimension of the polynomial space, which corresponds to the cardinality of the multi-index set Λ. For convenience, the set Λ can be arranged in lexicographical order, and according to this order, we can denote by $\mathbf{p}^j$ the j-th multi-index of Λ. Sometimes we refer to the elements of Λ with the generic multi-index $\mathbf{p}$, rather than listing them by the lexicographical index.

Since the monomial basis in (1) is very ill-conditioned, in practice we use an orthonormal polynomial basis. A typical choice is to take orthogonal polynomials with respect to the measure $\rho(\mathbf{Y})d\mathbf{Y}$. We introduce an N-dimensional orthonormal polynomial basis $\{l_j\}_{j=1}^{\#\Lambda}$ of $\mathbb{P}_\Lambda$ with respect to the weighted inner product

$$(u, v)_{L_\rho^2} = \int_\Gamma u(\mathbf{Y})v(\mathbf{Y})\rho(\mathbf{Y})\, d\mathbf{Y},$$

i.e. $(l_i, l_j)_{L_\rho^2} = \delta_{ij}$. Assumption 1 ensures that the orthonormal basis is complete in L_ρ^2 when $\Lambda = \mathbb{N}^N$.

In the particular case where the density factorizes as $\rho(\mathbf{Y}) = \prod_{n=1}^N \rho_n(Y_n)$ the basis can be constructed by tensorizing 1D orthogonal polynomials with respect to each weight ρ_n separately. Given n, let $\{\varphi_j^n(\cdot)\}_j$ be the orthogonal polynomials with respect to ρ_n.

The jth multi-index $\mathbf{p}^j \in \Lambda$ is associated to the corresponding jth multidimensional basis function by

$$l_j(\mathbf{Y}) = \prod_{n=1}^{N} \varphi_{p_n^j}^n(Y_n). \tag{2}$$

Thus, using the basis functions provided by (2), the definition (1) of $\mathbb{P}_\Lambda$ becomes

$$\mathbb{P}_\Lambda(\Gamma) = \mathrm{span}\{l_j, \ j = 1, \dots, \#\Lambda\}, \tag{3}$$

and of course $\dim(\mathbb{P}_\Lambda) = \#\Lambda$. Observe that in general (1) and (3) are equivalent only if the index set Λ satisfies the Monotonicity Property 1.

We consider a random sample $\mathbf{y}_1, \dots, \mathbf{y}_M$ (with independent variables) of size $M \geq \#\Lambda$ of the random variable $\mathbf{Y}$, and then evaluate the function ϕ point-wise at each value $\mathbf{y}_i$, $i = 1, \dots, M$.

Finally, we compute a discrete least square approximation of the values $\phi(\mathbf{y}_i)$ in the polynomial space $\mathbb{P}_\Lambda$, i.e.

$$\phi_\Lambda = \Pi_M^{\Lambda,\omega}\phi = \underset{v \in \mathbb{P}_\Lambda(\Gamma)}{\mathrm{argmin}} \frac{1}{M} \sum_{i=1}^{M} (\phi(\mathbf{y}_i) - v(\mathbf{y}_i))^2. \tag{4}$$

We will use the superscript (or subscript) ω to denote a quantity that depends on the random sample $\mathbf{y}_1, \dots, \mathbf{y}_M$ (and therefore is random itself).

We now introduce the *random* discrete inner product

$$(u, v)_{M,\omega} = \frac{1}{M} \sum_{i=1}^{M} u(\mathbf{y}_i)v(\mathbf{y}_i), \tag{5}$$

that induces on Γ the corresponding discrete norm $\|u\|_{M,\omega} = (u, u)_{M,\omega}^{1/2}$. With this notation we can write (4) as

$$\text{find } \Pi_M^{\Lambda,\omega}\phi \in \mathbb{P}_\Lambda(\Gamma) \quad \text{s.t.} \quad (\phi - \Pi_M^{\Lambda,\omega}, v)_{M,\omega} = 0, \quad \forall v \in \mathbb{P}_\Lambda(\Gamma).$$

2.1 Common multivariate polynomial spaces

Some of the most common choices of function spaces are Tensor Product, Total Degree, and Hyperbolic Cross, which are defined by the index sets below. We index the set Λ by the subscript w, that denotes the maximum polynomial degree used:

$$\textbf{Tensor Product (TP)}, \quad \Lambda_w = \left\{ \mathbf{p} \in \mathbb{N}^N : \max_{n=1,\dots,N} p_n \leq w \right\}, \tag{6}$$

$$\textbf{Total Degree (TD)}, \quad \Lambda_w = \left\{ \mathbf{p} \in \mathbb{N}^N : \sum_{n=1}^{N} p_n \leq w \right\}, \tag{7}$$

$$\textbf{Hyperbolic Cross (HC)}, \quad \Lambda_w = \left\{ \mathbf{p} \in \mathbb{N}^N : \prod_{n=1}^{N} (p_n + 1) \leq w + 1 \right\}. \tag{8}$$

These spaces are isotropic in the sense that the maximum polynomial degree w is the same in all variables $Y_1, \dots, Y_N$. The dimensions of TP and TD spaces are

$$\#TP(w, N) = (w + 1)^N, \tag{9}$$

$$\#TD(\mathrm{w}, N) = \binom{N + \mathrm{w}}{N}. \tag{10}$$

The dimension of the HC space is harder to quantify, so we report its exact dimension $\#HC(\mathrm{w}, N)$ in Fig. 1, computed for some values of w and N. An upper bound is given by

$$\#HC(\mathrm{w}, N) \leq \left\lfloor (\mathrm{w} + 1) \cdot (1 + \log(\mathrm{w} + 1))^{N-1} \right\rfloor. \tag{11}$$

This bound is sharp for $N = 2$ and becomes very conservative as N increases.
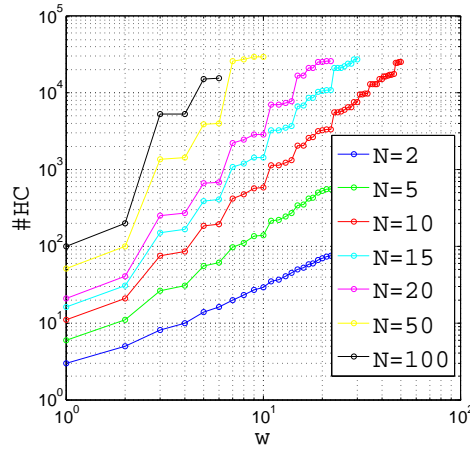
Figure 1: Dimension of the HC space, $N = 2, 5, 10, 15, 20, 50, 100$.

2.2 Stability and convergence rate of the random discrete L^2 projection

Here we recall some theoretical results concerning the discrete L^2 projection, derived in [14] and [5]. Let us first introduce the following quantity

$$C^\omega(M, \Lambda) := \sup_{v \in \mathbb{P}_\Lambda \setminus \{v \equiv 0\}} \frac{\|v\|_{L_\rho^2}^2}{\|v\|_{M,\omega}^2}, \tag{12}$$

that depends on the random sample and is therefore a random variable. The following proposition states the optimality of the discrete L^2 projection with respect to the L^∞ norm, when the error is evaluated in the L_ρ^2 norm, that is:

Proposition 1 (see [14]) *With $C^\omega(M, \Lambda)$ defined as in (12), it holds*

$$\|\phi - \Pi_M^{\Lambda, \omega} \phi\|_{L_\rho^2} \leq \left(1 + \sqrt{C^\omega(M, \Lambda)} \right) \inf_{v \in \mathbb{P}_\Lambda(\Gamma)} \|\phi - v\|_{L^\infty}. \tag{13}$$

As a consequence, the convergence properties of the random discrete projection are strictly related to the properties of the quantity $C^\omega(M, \Lambda)$. The next theorem quantifies the asymptotic behaviour of the random variable $C^\omega(M, \Lambda)$.

Theorem 1 (see [14]) *Let $C^\omega(M, \Lambda)$ be the random variable defined in (12). Then, for any given Λ we have*

$$\lim_{M \to \infty} C^\omega(M, \Lambda) = 1, \quad a.s.$$

The previous proposition and theorem are general results on the discrete L^2 projection: they hold in any dimension N, for any arbitrary N-dimensional monotone multi-index set Λ, and for any density ρ.

When $N = 1$ and $\rho = \mathbb{U}([-1, 1])$ a probability estimate has been proved in [14]. In this particular case the polynomial space is denoted by $\mathbb{P}_\text{w}$ rather than $\mathbb{P}_\Lambda$, because the multi-index set Λ is just $\{1, \dots, \text{w}\}$ and its dimension $\#\Lambda = 1 + \text{w}$. The following theorem ensures the stability and accuracy of the discrete L^2 projection, under the condition $M \propto (\#\Lambda)^2$:

Theorem 2 ([14]) *For any $\alpha \in (0, 1)$, under the condition*

$$\frac{M}{3 \log((M+1)/\alpha)} \geq 4\sqrt{3}\,\text{w}^2 \tag{14}$$

it holds

$$\mathbb{P}\left(\|\phi - \Pi_M^{\text{w};\omega}\phi\|_{L_\rho^2} \leq \left(1 + \sqrt{3 \log \frac{M+1}{\alpha}}\right) \inf_{v \in \mathbb{P}_\text{w}} \|\phi - v\|_{L^\infty}\right) \geq 1 - \alpha. \tag{15}$$

We remark that in practice condition (14) is equivalent to $M \propto (\#\Lambda)^2$, since the effect due to the presence of the nonoptimal logarithmic factor is often negligible. In [5] an estimate in expectation for the error $\|\phi - \Pi_M^{\text{w};\omega}\phi\|_{L_\rho^2}$ has also been derived, showing that it behaves as the L^2 best approximation error under the same condition $M \propto (\#\Lambda)^2$.

There exists also a general relation between the optimal convergence rate of the random projection and its stability, which holds again in any dimension N and for any Λ and ρ. The same random variable C^ω, besides entering in the error estimate (13), plays a role in the stability of the random projection, as stated in the next proposition. As in [14], we denote by D^ω the random design matrix associated to problem (4); its elements are defined as $[D^\omega]_{i,j} = l_j(\mathbf{y}_i)$.

Proposition 2 (From [14]) *The spectral condition number (2-norm) of the matrix $(D^\omega)^T D^\omega$ is equal to*

$$K\left((D^\omega)^T D^\omega\right) = c^\omega(M, \Lambda)\, C^\omega(M, \Lambda), \tag{16}$$

where

$$c^\omega(M, \Lambda) := \sup_{v \in \mathbb{P}_\Lambda \setminus \{v \equiv 0\}} \frac{\|v\|_{M,\omega}^2}{\|v\|_{L_\rho^2}^2}. \tag{17}$$

3   Parametric PDEs

In [14] we presented some numerical examples of RDP to approximate monovariate and multivariate target functions $\phi = \phi(\mathbf{Y}) : \Gamma \to \mathbb{R}$ on polynomial spaces. The role of smoothness was investigated. When using a relation $M \propto (\#\Lambda)^2$ an optimal convergence rate was always observed. On the other hand, when using a linear relation $M \propto \#\Lambda$ the optimal convergence rate was observed up to a certain threshold, after which the

error starts increasing and eventually diverges. This effect was clearly observed in the monovariate case. However, in higher dimensions the blow up of the error was not observed in the range of practical polynomial degrees explored. As pointed out in [14], the linear relation $M \propto \#\Lambda$ seems therefore to be sufficient for all practical purposes to achieve an accurate and stable approximation.

The aim of this paper is to test the RDP when the target function ϕ is related to the solution of a stochastic PDE model. We focus on Quantities of Interest of integral type over the spatial domain of the PDE model, such as the mean of the solution in portions of the domain, the mean energy of the solution, or point-wise quantities such as the maximum or minimum of the solution in the domain.

Consider a steady state PDE model,

$$\mathcal{L}(\mathbf{y}, u, f, g, \Omega) = 0, \tag{18}$$

defined on a bounded domain $\Omega \subset \mathbb{R}^d$ and parametrized by $\mathbf{y} \in \Gamma \subseteq \mathbb{R}^N$, with $u : \Omega \times \Gamma \to \mathbb{R}$ its solution, $f : \Omega \times \Gamma \to \mathbb{R}$ the forcing term, and $g : \partial\Omega \times \Gamma \to \mathbb{R}$ a suitable boundary condition. The following examples feature only two-dimensional spatial domains Ω, *i.e.* $d = 2$. However, extensions to 3D problems are straightforward. For the sake of notation, we will hereafter omit the dependence on the independent variable $\mathbf{x} \in \Omega$. The domain may also depend on the parameter $\mathbf{y}$, *i.e.* $\Omega = \Omega(\mathbf{y})$. Moreover, we assume that f and g satisfy proper conditions to make the whole model well-posed in the sense of Hadamard.

Considering $\mathbf{y}$ as a realization of the random variable $\mathbf{Y} \in \Gamma$ distributed according to the density $\rho : \Gamma \to \mathbb{R}^+$, the parametric model (18) can also be considered as a PDE model with stochastic data.

We now proceed with some examples to illustrate the application of the RDP to approximate Quantities of Interest depending on the solution of stochastic PDE's. First we focus on models in the elliptic class, where the solution typically depends smoothly on the random variable, as proved in [6, 1].

The first three examples concern the Darcy flow in a medium containing some inclusions. The first and second examples have a one-dimensional stochastic parameter space: in Example 1 the value of the diffusion coefficient is stochastic, while in Example 2 the geometrical shape of the inclusion is stochastic. In Example 3 we increase the dimension of the parameter space to five.

Then we analyze the linear elasticity model and the incompressible Navier-Stokes model. The former exhibits a highly regular dependence of the solution on the random parameter affecting the *Young's modulus*, while the latter shows some non-smooth QOIs.

To quantify the error $\|\phi - \Pi_M^{\Lambda,\omega}\phi\|_{L_\rho^2}$ committed by RDP we employ the cross-validation procedure described in [14, Section 4]. In all the numerical tests we choose 100 cross-validation points. The stability of the random projection is quantified by the (2-norm) condition number of the design random matrix D^ω, as in [14, Section 4]. In the convergence plots, the continuous lines mark the mean of the error $\|\phi - \Pi_M^{\Lambda,\omega}\phi\|_{L_\rho^2}$, or the mean of the condition number of the random design matrix, while the dashed line mark the mean plus one standard deviation. The discretization of the PDE model over the spatial domain Ω is obtained by means of the Finite Element method. In Examples 1,2,3,4 the P1 finite elements are used. In Example 5 the *inf-sup* compatible P2-P1 finite elements are used.

3.1 Example 1: the Darcy flow in a domain with one inclusion

To start with, we consider an elliptic model on a bounded deterministic domain $\Omega \subset \mathbb{R}^2$, with a random diffusion coefficient μ:

$$\begin{cases} -\nabla \cdot (\mu(\mathbf{x}, \mathbf{y}) \nabla u(\mathbf{x}, \mathbf{y})) = 0, & \mathbf{x} \text{ in } \Omega, \ \mathbf{y} \in \Gamma, \\ u(\mathbf{x}, \mathbf{y}) = g_1(\mathbf{x}), & \mathbf{x} \text{ on } \partial\Gamma_1 \cup \partial\Gamma_3, \ \mathbf{y} \in \Gamma, \\ \partial_\nu u(\mathbf{x}, \mathbf{y}) = g_2(\mathbf{x}), & \mathbf{x} \text{ on } \partial\Gamma_2 \cup \partial\Gamma_4, \ \mathbf{y} \in \Gamma. \end{cases} \tag{19}$$

We set problem (19) in a unitary square domain, with a circular inclusion Ω_I with radius 0.2, as shown in Fig. 2. The edges are labeled clockwise as $\Gamma_1, \Gamma_2, \Gamma_3, \Gamma_4$ starting from the left. We impose nonhomogeneous Dirichlet conditions on the vertical edges,
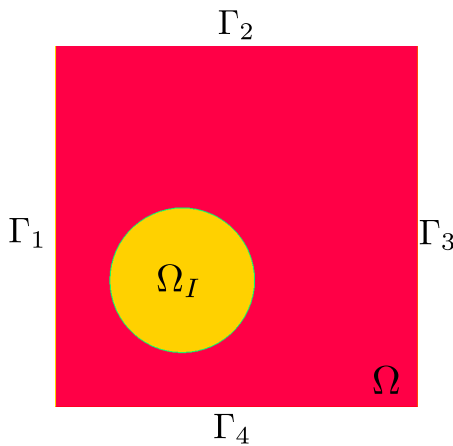
Figure 2: Square domain Ω with a circular inclusion Ω_I.

and homogeneous Neumann conditions on the horizontal ones, so to force a steady state flow from left to right. The random diffusion coefficient depends on a uniform random variable $Y \sim \mathcal{U}(-1, 1)$, and is defined as

$$\mu(\mathbf{x}, Y) = \begin{cases} \exp(5\,Y), & \Omega_I, \\ 10^{-4}, & \Omega \setminus \Omega_I. \end{cases} \tag{20}$$

Such a model for the coefficient can be employed in practical situations where the value of the diffusion properties of the material are not accurately determined in a given region of the physical domain, or when the value is a function of the outcome of some stochastic process with a known underlying probability law. Notice that the aforementioned diffusion coefficient may jump by more than 4 orders of magnitude from the bulk to the inclusion.

The QOIs we analyze are defined by integrals of the solution over the physical domain. We consider the mean of the solution u in Ω,

$$\mathrm{QOI}_1(u) = \frac{1}{|\Omega|} \int_\Omega u \, dx, \tag{21}$$

the mean of $|\nabla u|^2$ in Ω

$$\mathrm{QOI}_2(u) = \frac{1}{|\Omega|} \int_\Omega |\nabla u|^2 \, dx, \tag{22}$$

and the mean of the solution on the left boundary segment Γ_1,

$$\text{QOI}_3(u) = \frac{1}{|\Gamma_1|} \int_{\Gamma 1} u \, dx. \tag{23}$$

The numerical results obtained with a sample size chosen as $M \propto \#\Lambda$ are reported in Fig. 3. When the value of the proportionality constant c decreases too much, the convergence rate achieved by the random projection is reduced, and the variability of the error amplifies as well. Analogous results were shown in [14] for scalar target functions.

The optimal convergence rate in terms of w is shown in Fig. 4-left, obtained using the quadratic rule $M \propto (\#\Lambda)^2$. Note that the rule $M = 20 \cdot \#\Lambda$ used in Fig. 3 uses more points than the rule $M = (\#\Lambda)^2$ for the range of polynomial degrees considered. So the corresponding curve in Fig. 3 can also be considered as the optimal convergence rate. In addition, Theorem 2 tells us that with $M \propto (\#\Lambda)^3$ we would converge with
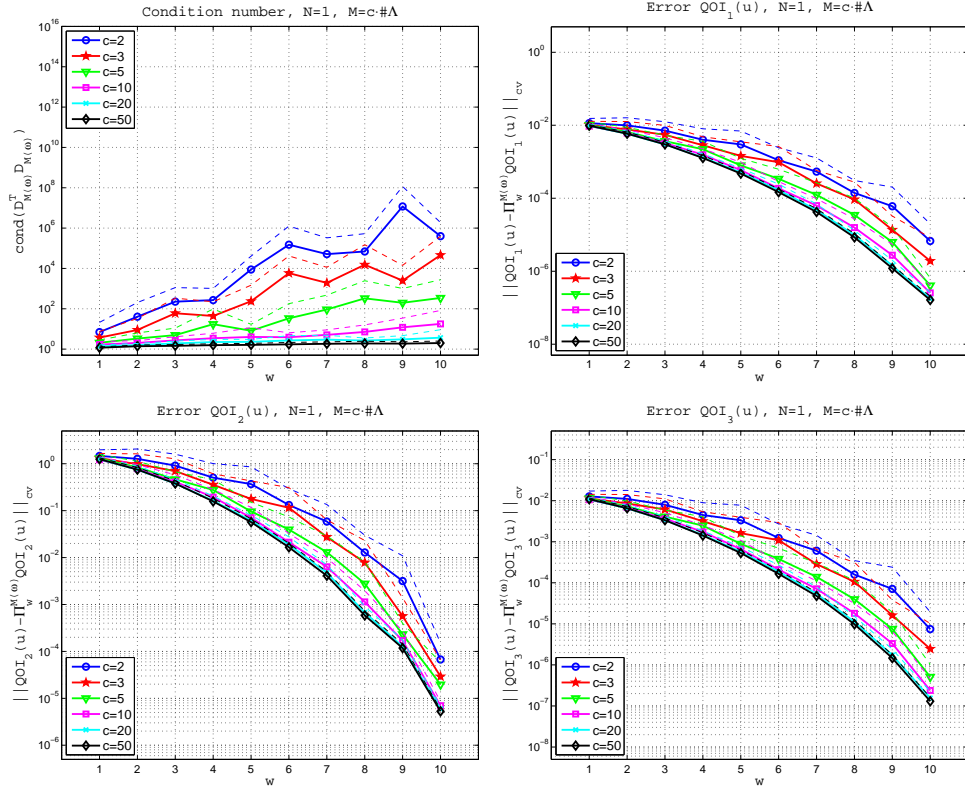
Figure 3: Example 1. Condition number and approximation errors averaged over 100 repetitions, $M = c \, \#\Lambda$.

the same optimal rate given by $M \propto (\#\Lambda)^2$. This is confirmed numerically, since the convergence rates in Fig. 4-right and Fig. 4-left are the same.

To simplifly the comparison among the results obtained with $M \propto \#\Lambda$, $M \propto (\#\Lambda)^2$, and $M \propto (\#\Lambda)^3$ we summarize the convergence plots in Fig. 5 putting M instead of w on the abscissas. The optimal convergence rate, *e.g.* obtained with $M = 1 \cdot (\#\Lambda)^2$, is exponentially fast and monotonous w.r.t. the sample size M. Choosing a smaller
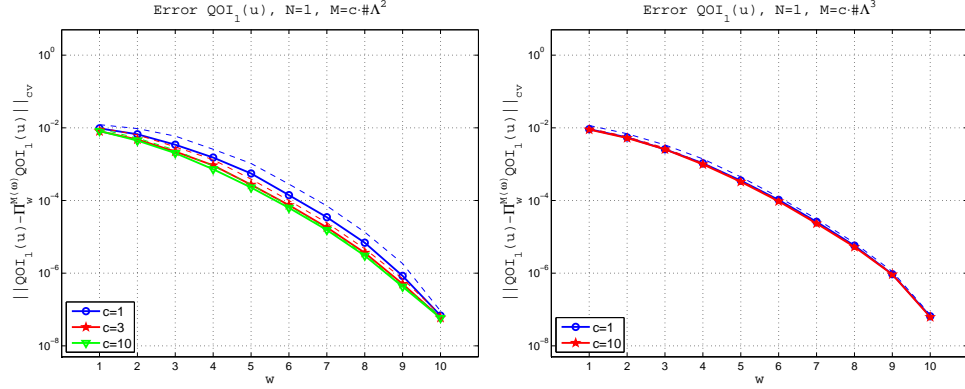
Figure 4: Example 1. Approximation errors averaged over 100 repetitions, $M = c \cdot (\#\Lambda)^2$ (left), $M = c \cdot (\#\Lambda)^3$ (right).

sample size, *e.g.* $M = 2 \cdot \#\Lambda$, yields a faster convergence up to a certain threshold, after which the solution deteriorates. This effect is also seen in [14, Fig.8].
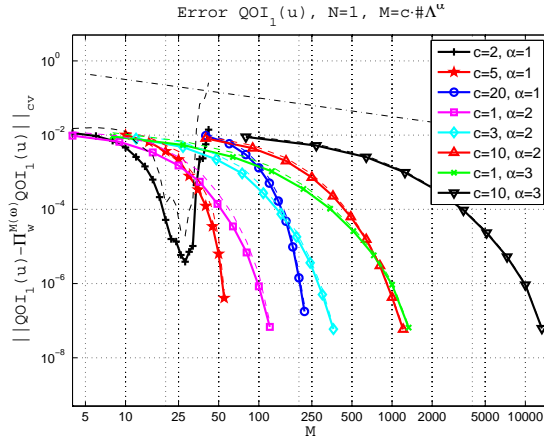
Figure 5: Example 1. Approximation errors vs M for different choices of the sample size, $M = c \cdot (\#\Lambda)^\alpha$. Same data as in Fig. 3 (top-right) and Fig. 4.

3.2 Example 2: the Darcy model in a domain with an inclusion of random shape

The second example we consider is based on problem (19), but now we choose a deterministic value of the diffusion coefficient μ as

$$\mu(\mathbf{x}, \mathbf{Y}) = \begin{cases} 1, & \Omega_I, \\ 10^{-6}, & \Omega \setminus \Omega_I, \end{cases} \tag{24}$$

and the randomness is in the radius of the circular inclusion Ω_I, which is centered in $(0.4, 0.4)$ and has a radius R which is determined by the uniform random variable

$Y \sim \mathcal{U}(-1, 1)$ as $R = (Y+2)/10$. For each realization of the random variable we remesh the whole domain. The motivations for this example are to investigate the effect of a discontinuity of the diffusion coefficient with random location in the physical domain. The discontinuity consists in the boundary of the inclusion where the diffusion coefficient jumps by six orders of magnitude. The QOIs considered are the same as in Example 1.
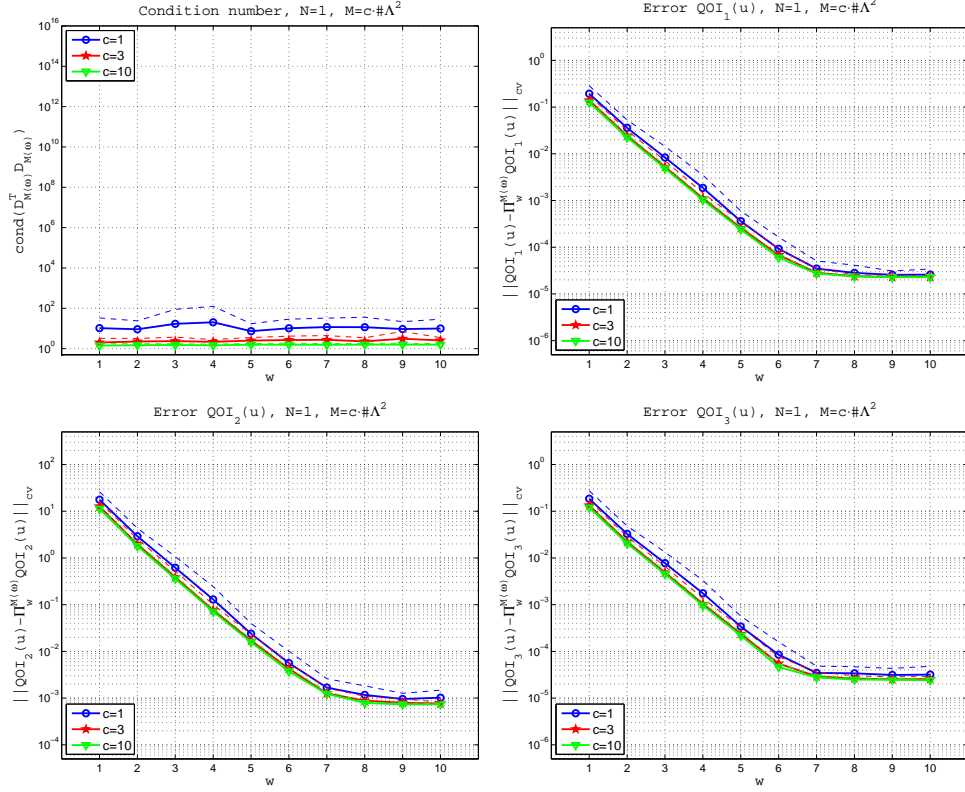
Figure 6: Example 2. Condition number and approximation errors averaged over 100 repetitions, $M = c \cdot (\#\Lambda)^2$.

In Fig. 6 we observe an exponential convergence up to w = 6 for all the three QOIs, and this example shows that there are smooth QOIs even if the problem presents discontinuities with a random location (hence the solution itself, measured in the $L^2(\Omega)$ or $H^1(\Omega)$ norm, is not smooth with respect to **Y**). For larger values than w = 6 the error levels out due to not negligible contributions of the finite element error.

We notice from Fig. 6 that the convergence plots for $M = 3 \cdot (\#\Lambda)^2$ and $M = 10 \cdot (\#\Lambda)^2$ are nearly identical. Therefore already $M = 3 \cdot (\#\Lambda)^2$ gives the optimal rate in terms of w. We have also checked the cubic relation $M = \#\Lambda^3$ (Fig.6-right).

We have verified that a similar convergence behavior holds when varying the value of the diffusion coefficient in the bulk, or when considering quantities of interest such as the integral over a line that always intersects the inclusion.

Example 2: a less smooth QOI We now build a QOI that exhibits a less regular dependence on the random variable $\mathbf{Y}$. We consider again problem (19) with the value of the diffusion coefficient μ given by

$$\mu(\mathbf{x}, \mathbf{Y}) = \begin{cases} 1, & \Omega_I, \\ 10^{-2}, & \Omega \setminus \Omega_I, \end{cases} \tag{25}$$

and the circular inclusion Ω_I with random radius as in the previous section. Note that the discontinuity of the coefficient is a jump of two orders of magnitude across the boundary of the inclusion. Now we consider the following quantities of interest,

$$\mathrm{QOI}_4(\mathbf{Y}) = u(\widetilde{\mathbf{x}}, \mathbf{Y})\Big|_{\widetilde{\mathbf{x}}=(0.4,0.4)}, \qquad \mathrm{QOI}_5(\mathbf{Y}) = u(\widetilde{\mathbf{x}}, \mathbf{Y})\Big|_{\widetilde{\mathbf{x}}=(0.55,0.55)}, \tag{26}$$

that are point-wise evaluations of the solution u of problem (19) in two fixed positions $\widetilde{\mathbf{x}} = (0.4, 0.4)$ and $\widetilde{\mathbf{x}} = (0.55, 0.55)$. The former coincides with the center of the random shape inclusion, and therefore always lies inside it. The latter point may or may not belong to the inclusion, depending on the outcome of the random variable $\mathbf{Y}$ that determines the radius of the inclusion. The corresponding results are displayed in Fig. 7. The QOI associated to the point $\widetilde{\mathbf{x}} = (0.4, 0.4)$ exhibits a faster convergence than the one associated to $\widetilde{\mathbf{x}} = (0.55, 0.55)$, since the discontinuity in the coefficient affects the regularity of the solution exactly in the point where it is evaluated. In this case, the point $\widetilde{\mathbf{x}} = (0.55, 0.55)$ is such that the probability to fall inside the inclusion is approximately twice the probability to fall outside it. Of course there are also QOIs that are hard to approximate: *e.g.* the one associated to the point $\widetilde{\mathbf{x}} = (0.6, 0.6)$ that falls inside the inclusion with a probability larger than 98%. In this case the use of *importance sampling* techniques (see *e.g.* [15]) should be considered.
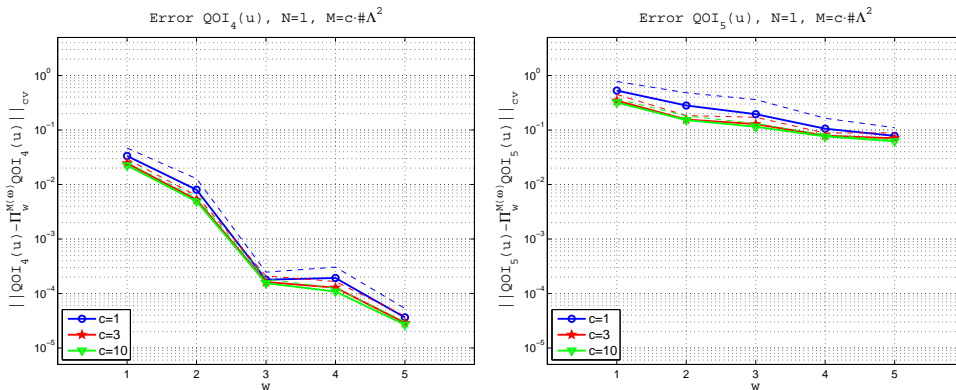
Figure 7: Example 2. Approximation errors averaged over 100 repetitions, $M = c \cdot (\#\Lambda)^2$.

3.3 Example 3: the Darcy flow in a domain with five inclusions

In the next test we again use problem (19), and increase the dimension of the parameter space Γ to $N = 5$ by adding some inclusions, as shown in Fig. 8. The inclusions are circular with radius equal to 0.1, and are centered in the points $\mathbf{x} = (0.5, 0.5)$ and

$\mathbf{x} = (0.5 \pm 0.25, 0.5 \pm 0.25)$. We denote by Ω_i, $i = 1, \ldots, 5$, the inclusion domains and with $\Omega_0 = \Omega \setminus \cup_{i=1}^{5} \Omega_i$ the bulk. Therefore $\Omega = \left(\bigcup_{i=0}^{5} \Omega_i \right)$, and the sets Ω_i are not overlapping each other. The random diffusion coefficient depends now on a multivariate uniform random variable $\mathbf{Y} \sim \mathcal{U}([-1, 1]^5)$, and is defined as

$$\mu(\mathbf{x}, \mathbf{Y}) = \begin{cases} \exp(\beta \, Y_i), & \Omega_i, \quad i = 1, \ldots, 5, \\ 10^{-4}, & \Omega_0, \end{cases} \tag{27}$$

such that each random variable is associated to an inclusion. We consider the same quantities of interest as in Example 1. The chosen polynomial space $\mathbb{P}_\Lambda$ is the isotropic Total Degree space. This choice is motivated by the analysis in [2]. We set $\beta = 2$, so that the coefficient variations in the inclusions are of two orders of magnitude, and report the results in Fig. 9. The convergence rate is exponential whenever the value of c is larger than 1. A number of points $M = 3 \cdot \#\Lambda$ is enough to achieve the optimal convergence rate, and no deterioration is observed up to the maximal polynomial degree w = 10 considered. Then we set $\beta = 5$ and obtain the results in Fig. 10. Note that this case yields a variation of more than 4 orders of magnitude in the coefficient inside the inclusions. As a consequence we observe that the convergence remains exponential, but with a slower rate.
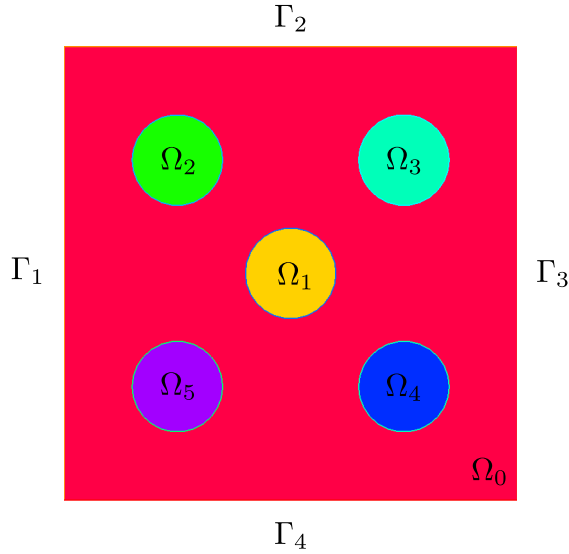
Figure 8: Domain with 5 inclusions $\Omega_1, \Omega_2, \Omega_3, \Omega_4, \Omega_5$ with random diffusivity for problem (19).
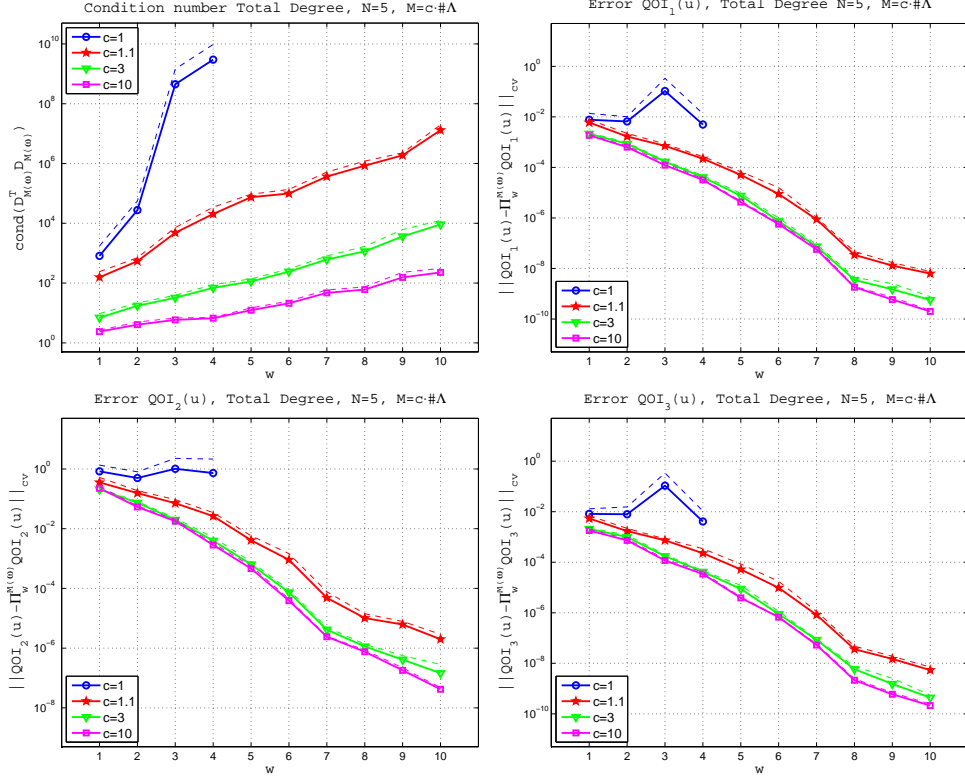
Figure 9: Example 3: the Darcy model. $\beta = 2$.
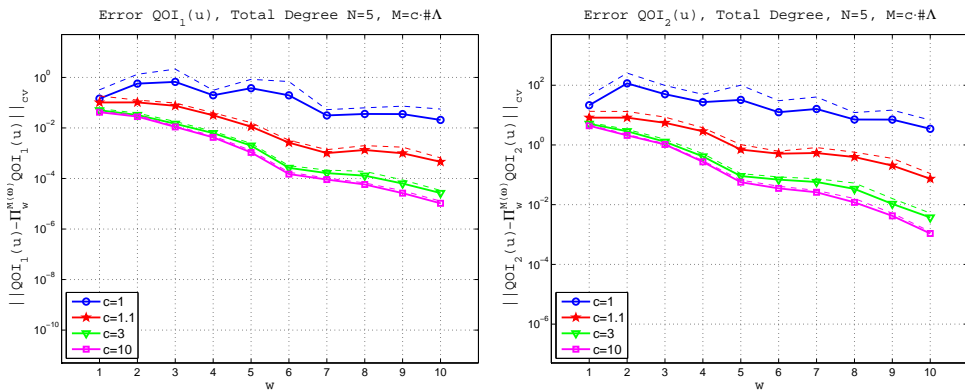
Figure 10: Example 3: the Darcy model. $\beta = 5$.

3.4 Example 4: the cantilever beam

We consider the *Navier-Lamé* equation written in displacement form on the domain $\Omega = \cup_{i=1}^{7}\Omega_i$ depicted in Fig. 11:

$$\begin{cases} -(\lambda(\mathbf{x},\mathbf{Y}) + \mu(\mathbf{x},\mathbf{Y}))\nabla(\nabla \cdot \mathbf{u}) + \mu(\mathbf{x},\mathbf{Y})\nabla^2\mathbf{u} = -f(\mathbf{x},\mathbf{Y}), & \mathbf{x} \in \Omega, \, \mathbf{Y} \in \Gamma, \\ \sigma(\mathbf{u}) \cdot \mathbf{n} = 0, & \mathbf{x} \text{ on } \partial\Omega \setminus \Gamma_{wall}, \, \mathbf{Y} \in \Gamma, \\ \mathbf{u} = \mathbf{0}, & \mathbf{x} \text{ on } \Gamma_{wall}, \, \mathbf{Y} \in \Gamma, \end{cases} \tag{28}$$

with

$$\mu(\mathbf{x},\mathbf{Y}) = \frac{E(\mathbf{x},\mathbf{Y})}{2(1+\nu)}, \qquad \lambda(\mathbf{x},\mathbf{Y}) = \frac{\nu\,E(\mathbf{x},\mathbf{Y})}{(1+\nu)(1-2\,\nu)},$$

and with σ the usual stress tensor

$$\sigma(\mathbf{u}) = \lambda(\nabla \cdot \mathbf{u})\mathbf{I} + 2\,\mu\,\frac{\nabla\mathbf{u} + \nabla^T\mathbf{u}}{2}.$$

The *Young's modulus* E is affected by uncertainty, and it depends on the random variable $\mathbf{Y} \sim \mathcal{U}([-1,1]^7)$ in the following way:

$$E(\mathbf{x},\mathbf{Y}) = \exp(7 + Y_i), \text{ in } \Omega_i, \qquad i = 1,\ldots,7.$$

The *Poisson's ratio* ν is deterministic and equal to 0.28. The prescribed boundary conditions are null displacement on Γ_{wall} and null stress on $\partial\Omega \setminus \Gamma_{wall}$. The forcing term $f \equiv -1$ models the distributed action of the gravity force. The reference configuration of the cantilever is a one-by-seven rectangle. Further details about the geometry are given in Fig. 11. As in Example 3, we choose $\mathbb{P}_\Lambda$ to be the isotropic Total Degree space. We are interested in the following quantities of interest

$$\text{QOI}_6(\mathbf{u}) = \int_\Omega |\nabla u_1|^2 + |\nabla u_2|^2 \, d\mathbf{x},$$

$$\text{QOI}_7(u_2) = \min_{\mathbf{x}\in\Omega} u_2(\mathbf{x}), \qquad \text{QOI}_8(\mathbf{u}) = \int_\Omega \sigma_{12}(\mathbf{u}) \, d\mathbf{x}.$$

In Fig. 12 we report the corresponding results. The convergence is exponential even with $M = 1.1 \cdot \#\Lambda$, that is very close to the minimal number of points required to have an overdetermined problem. The red line corresponds to the choice $M = 3 \cdot \#\Lambda$, and can be considered the optimal convergence rate, since no improvement is observed when going to $M = 10 \cdot \#\Lambda$ (green line).

3.5 Example 5: Navier-Stokes equations in a random domain

In the last example, we consider the steady state incompressible Navier-Stokes equations which govern the motion of a fluid in a pipe:

$$\begin{cases} -\nu\Delta\mathbf{u} + \left(\mathbf{u} \cdot \nabla\right)\mathbf{u} + \nabla p = 0, & \text{in } \Omega, \\ \nabla \cdot \mathbf{u} = 0, & \text{in } \Omega, \\ +\text{B.C.} & \text{on } \partial\Omega. \end{cases} \tag{29}$$

The presence of uncertainty in the model is described by a two-dimensional uniform random variable $\mathbf{Y} \sim \mathcal{U}([-1,1]^2)$. The first component Y_1 models the uncertainty in
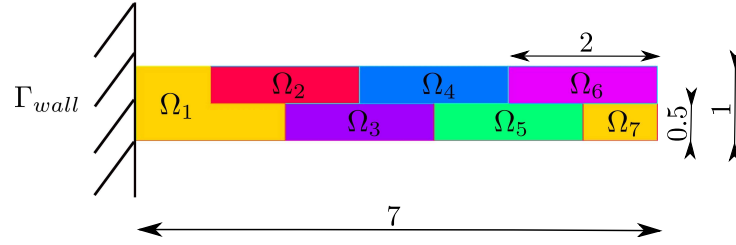
Figure 11: The cantilever beam.
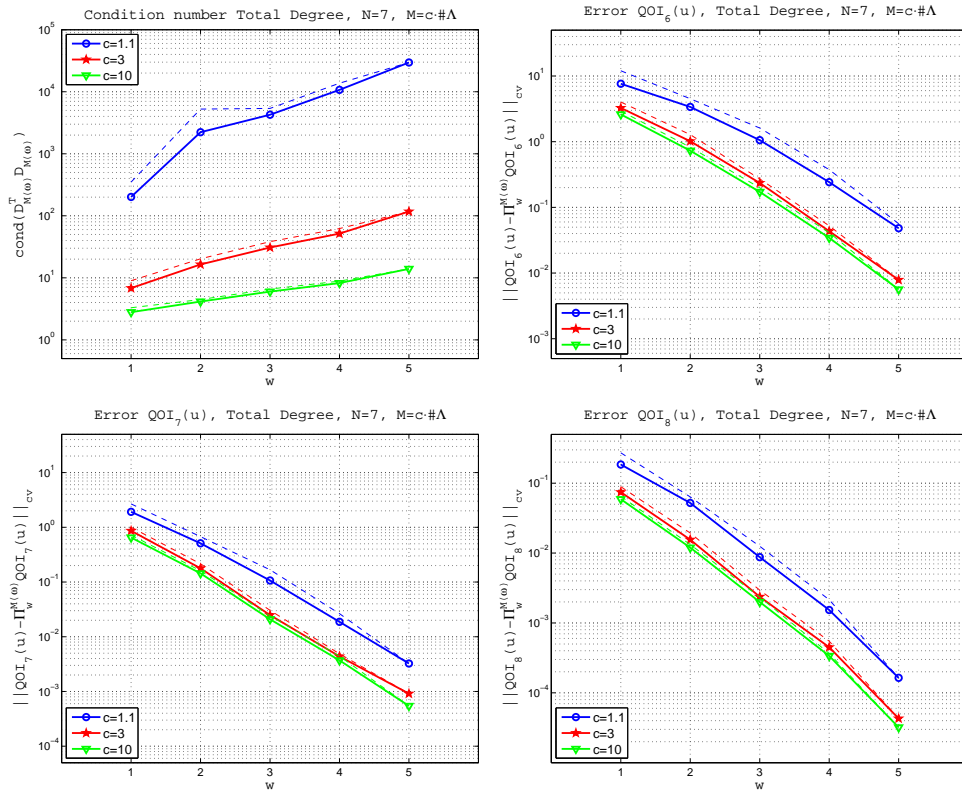
Figure 12: Example 4. Condition number and approximation errors averaged over 100 repetitions, $M = c \cdot \#\Lambda$.

the diffusion coefficient $\nu(\mathbf{Y}) = 10^{-Y_1}$, while the second component determines the geometrical parameter r_1 by

$$r_1 = \frac{1.5 + Y_2}{5}.$$

The parameter r_1 defines the curvature in the innermost part of the elbow of the pipe. The parameter $r_2 = 0.3$ is kept fixed, since it has a minor influence on the solution of the model. The size of the inflow and outflow sections of the pipe and other geometrical details are reported in Fig. 13. We choose again $\mathbb{P}_\Lambda$ to be the isotropic Total Degree
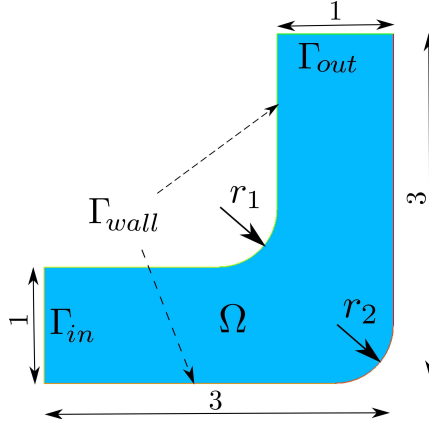
Figure 13: Geometry of the domain Ω in Example 5.

space, although the two random variables have clearly different roles. We impose a Poiseuille velocity profile on Γ_{in} with maximal velocity equal to 4, no-slip conditions on Γ_{wall}, null tangential velocity and null pressure on Γ_{out}. The quantities of interest that we address are given by the pressure as

$$\mathrm{QOI}_9(\mathbf{Y}) = \frac{1}{|\Gamma_{in}|} \int_{\Gamma_{in}} p(\mathbf{x}, \mathbf{Y}) \, d\mathbf{x}, \qquad \mathrm{QOI}_{10}(\mathbf{Y}) = p(\widetilde{\mathbf{x}}, \mathbf{Y})\Big|_{\widetilde{\mathbf{x}}=(2.5,1)},$$

and by the vorticity $\mathbf{v}(\mathbf{x}, \mathbf{Y}) = \nabla \times \mathbf{u}(\mathbf{x}, \mathbf{Y})$ as

$$\mathrm{QOI}_{11}(\mathbf{Y}) = \int_{\Omega} |\mathbf{v}(\mathbf{x}, \mathbf{Y})| \, d\mathbf{x}.$$

The point $\widetilde{\mathbf{x}} = (2.5, 1)$ lies in a central region of the domain where the pressure is largely affected by the values of the random parameters. The Reynolds number ranges from 0.4 to 40, depending on the realizations of the random variable $\mathbf{Y}$. The flow of the fluid is always in the laminar regime.

We report the numerical results obtained in Fig. 14. The QOIs associated to the pressure converge exponentially fast. On the other hand, the QOI with the vorticity is very sensitive to the input parameters. As a consequence, the corresponding QOI exhibits a slow convergence and the use of a high order polynomial approximation seems uneffective.
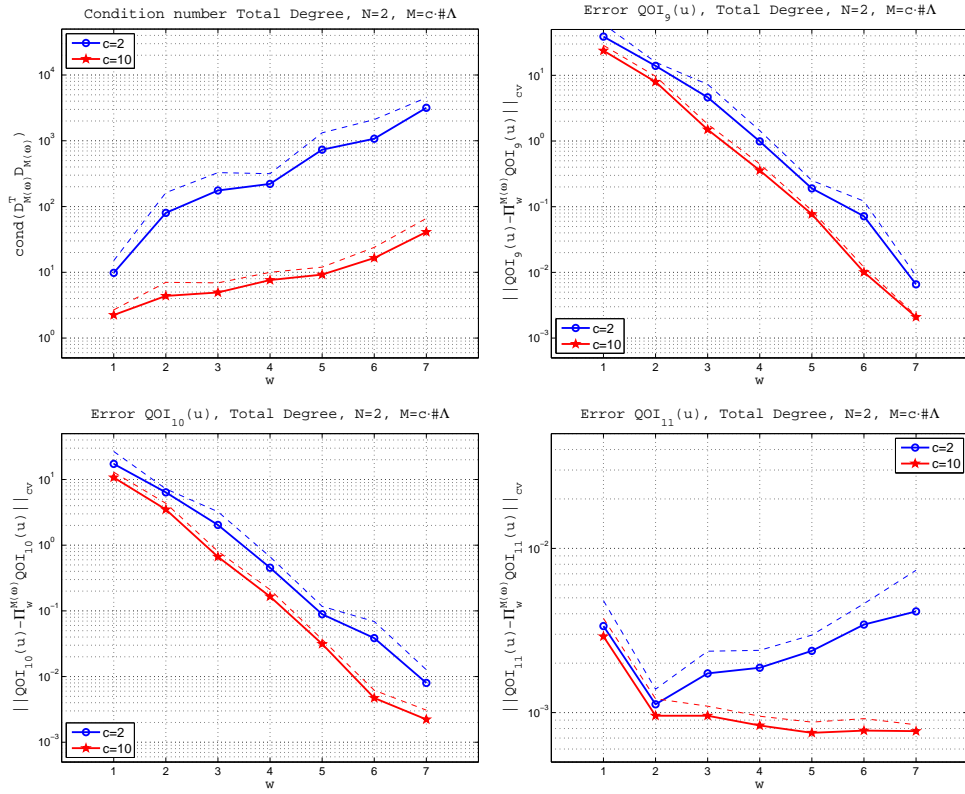
Figure 14: Example 5. Condition number and approximation errors averaged over 5 repetitions, $M = c \cdot \#\Lambda$.

4 Conclusions

In this work we have presented the use of RDP to approximate Quantities of Interest related to the solution of PDEs with stochastic data.

When the parameter space is one-dimensional, the stability and optimal convergence rate under the condition $M \propto (\#\Lambda)^2$ are ensured from the analysis proposed in [14]. We presented some results concerning two Darcy models, with values of the coefficient and geometrical shape of the inclusion governed by random variables, and showed numerically how the sample size affects the convergence rate, either using a rule with $M \propto \#\Lambda$ or a rule $M \propto (\#\Lambda)^2$.

Moreover, we have shown that in high dimensions the linear scaling $M \propto \#\Lambda$ yields an almost-optimal convergence rate, making the RDP particularly suited for the application to high dimensional problems. This behaviour of the RDP in high dimension is reported also in [14], where some numerical tests with scalar target functions are presented. In this work we tested many smooth QOIs related to the solution of the Darcy model, of the linear elasticity model, and of the Navier-Stokes equations.

In all cases exponential convergence has always been observed even with the linear fule $M \propto \#\Lambda$ and no deterioration of the convergence due to an insufficient sample size has been observed in the range of polynomial degrees tested. The only exception is Fig. 5 where for the rule $M = 2 \cdot \#\Lambda$ we had to reach w = 25 to start observing a deterioration. The situation is better in higher dimensions where no deterioration has been observed and the matrix $(D^\omega)^T D^\omega$ is better conditioned than in the monovariate case. Our conclusion is that for practical engineering applications, a linear rule $M = c \cdot \#\Lambda$ is acceptable, and the higher the dimension the smaller the constant can be taken.

We have also investigated the role that smoothness of the QOI w.r.t. the random variables plays in the convergence rate of RDP, including some examples of lower regularity QOI. For instance, we showed an example with a nonsmooth QOI related to the solution of the Darcy model and a QOI related to the vorticity of the solution of the incompressible Navier-Stokes equations. In both cases a subexponential convergence is observed. Other numerical tests with nonsmooth target functions are provided in [14].

The overall efficiency of RDP has to be compared with classical methods as Stochastic Galerkin and Stochastic Collocation on Sparse Grids. The RDP is more suited for applications than Stochastic Galerkin, since the evaluations of the target function are completely uncoupled and one might use a black box deterministic solver. In addition, RDP is very promising for intermediate to large dimensions and could be competitive or even better than Stochastic Collocation on Sparse Grids in terms of accuracy versus numbers of evaluations of the target function. A fair comparison between the two methods is out of the scope of the present paper, and will be addressed in a forthcoming work.

Acknowledgments

References

[1] I. Babuska, F. Nobile and R. Tempone, *A stochastic collocation method for elliptic partial differential equations with random input data*, SIAM Rev, 52 (2010), pp. 317–355.

[2] J. Beck and F. Nobile and L. Tamellini and R. Tempone, *Convergence of quasi-optimal stochastic Galerkin methods for a class of PDEs with random coefficients*, MATHICSE Technical Report 24.2012, École Polytechnique Fédérale de Lausanne (2012), submitted.

[3] B. Blatman and B. Sudret, *Sparse polynomial chaos expansions and adaptive stochastic finite elements using regression approach*, C.R.Mechanique 336:518–523, 2008.

[4] H. J. Bungartz and M. Griebel, *Sparse grids*, Acta Numerica, 13:147–269, 2004.

[5] A. Cohen, M.A. Davenport and D. Leviatan, *On the stability and accuracy of Least Squares approximations*, arXiv 1111.4422 (2011).

[6] A. Cohen, R. Devore and C. Schwab, *Analytic regularity and polynomial approximation of parametric and stochastic elliptic PDE's*, Anal. Appl. (Singap.), 9 (2011), pp. 11–47.

[7] M. Eldred, C. Webster and P. Constantine, *Evaluation of Non-Intrusive Approaches for Wiener-Askey Generalized Polynomial Chaos*, American Institute of Aeronautics and Astronautics, 2008.

[8] M. Eldred, *Design under uncertainty employing stochastic expansion methods*, International Journal for Uncertainty Quantification, 1:119–146, 2011.

[9] B. Ganapathysubramanian and N. Zabaras, *Sparse grid collocation schemes for stochastic natural convection problems*, J. Comput. Phys., 225: 652–685, 2007.

[10] R. Ghanem and P.D. Spanos, *Stochastic Finite Elements: a spectral approach*, Dover Publications, 2003.

[11] L. Gyorfi, M. Kohler, A. Krzyzak and H. Walk, *A distribution-free theory of nonparametric regression*, Springer-Verlag, 2002.

[12] S. Hosder, R. W. Walters and M. Balch, *Point-collocation nonintrusive polynomial chaos method for stochastic computational fluid dynamics*, AIAA Journal, 48:2721–2730, 2010.

[13] O. Le Maitre and O.M. Knio, *Spectral Methods for Uncertainty Quantification*, Springer, 2010.

[14] G. Migliorati, F. Nobile, E. von Schwerin and R. Tempone, *Analysis of the discrete L^2 projection on polynomial spaces with random evaluations*, MOX report 46-2011, Politecnico di Milano, Italy (2011), submitted.

[15] C. P. Robert and G. Casella, *Monte Carlo statistical methods*, Springer-Verlag, 2004.

[16] D. Xiu and G. E. Karniadakis, *The Wiener-Askey polynomial chaos for stochastic differential equations*, SIAM J. Sci. Comput., 24(2):619–644, 2002.

MOX Technical Reports, last issues

**Dipartimento di Matematica "F. Brioschi",
Politecnico di Milano, Via Bonardi 9 - 20133 Milano (Italy)**

49/2012 MIGLIORATI, G.;NOBILE, F.;VON SCHWERIN, E.;TEMPONE, R.
Approximation of Quantities of Interest in stochastic PDEs by the random discrete L2 projection on polynomial spaces

48/2012 GHIGLIETTI, A.; PAGANONI, A.M.
Statistical properties of two-color randomly reinforced urn design targeting fixed allocations

47/2012 ASTORINO, M.; CHOULY, F.; QUARTERONI, A.
Multiscale coupling of finite element and lattice Boltzmann methods for time dependent problems

46/2012 DASSI, F.; PEROTTO, S.; FORMAGGIA, L.; RUFFO, P.
Efficient geometric reconstruction of complex geological structures

45/2012 NEGRI, F.; ROZZA, G.; MANZONI, A.; QUARTERONI, A.
Reduced basis method for parametrized elliptic optimal control problems

43/2012 SECCHI, P.; VANTINI, S.; VITELLI, V.
A Case Study on Spatially Dependent Functional Data: the Analysis of Mobile Network Data for the Metropolitan Area of Milan

44/2012 FUMAGALLI, A.; SCOTTI, A.
A numerical method for two-phase flow in fractured porous media with non-matching grids

42/2012 LASSILA, T.; MANZONI, A.; QUARTERONI, A.; ROZZA, G.
Generalized reduced basis methods and n width estimates for the approximation of the solution manifold of parametric PDEs

41/2012 CHEN, P.; QUARTERONI, A.; ROZZA, G.
Comparison between reduced basis and stochastic collocation methods for elliptic problems

40/2012 LOMBARDI, M.; PAROLINI, N.; QUARTERONI, A.
Radial basis functions for inter-grid interpolation and mesh motion in FSI problems